

## Computer simulation of 3D electrical activity in the sinoatrial node

R. A. SYUNYAEV<sup>\*†</sup> and R. R. ALIEV<sup>\*†</sup>

**Abstract** — We have simulated 3D propagation of the action potential in the sinoatrial node to study the dynamics of the heart rhythm initiation. We have found that the leading center inside the sinoatrial node is formed by a group of cells, appears spontaneously under normal conditions, and migrates as acetylcholine is applied. The leading center drifts toward the center of the sinoatrial node, if we consider the effect of the surrounding atrial tissue. Abnormal electrical activity, rotating waves of action potential are observed in the sinoatrial node.

### 1. Mathematical model

We have simulated the electrical activity of cardiocytes based on the Hodgkin-Huxley formalism:

$$\frac{dU}{dt} = -\frac{1}{c_m} \sum I_i \quad (1.1a)$$

$$I_i = g_i \left( \prod \alpha_{ij} \right) (U - E_i(C)) \quad (1.1b)$$

$$\frac{d\alpha}{dt} = \frac{\alpha_\infty(U, C, p) - \alpha}{\tau(U, C, p)} \quad (1.1c)$$

$$E = \frac{RT}{zF} \log \left( \frac{C_o}{C_i} \right) \quad (1.1d)$$

Here,  $U$  is the transmembrane potential;  $c_m$  is the membrane capacity;  $I_i$  – transmembrane currents;  $g_i$  – maximum ion channel conductivities;  $\alpha_{ij}$  – gating variables;  $E_i$  – Nernst potentials;  $C$  – ion concentrations;  $p$  – other parameters (acetylcholine (ACh) concentration);  $C_o$  and  $C_i$  – ion concentrations outside and inside the cell, respectively;  $R$  – gas constant;  $T$  – temperature;  $z$  – ion charge;  $F$  – Faraday constant. The first equation (1.1a) relates the change in the transmembrane potential  $U$  to the sum of transmembrane currents; the second one describes the dynamics of ion currents close to the thermodynamic equilibrium (Ohm’s law) (1.1b); the third

<sup>\*</sup>Institute of Theoretical and Experimental Biophysics, Puschino, Moscow Region, 142290 Russia

<sup>†</sup>Moscow Institute of Physics and Technology, Dolgoprudnyi, Moscow Region, 141700 Russia

The work was supported by the Russian Foundation for Basic Research (10-04-01311).

one (1.1c) is the dynamics of gating variables proposed by Hodgkin and Huxley [8]; in a modern interpretation the equation describes the evolution of the probability of opening and closing of ion channels; the fourth one (1.1d) is the Nernst potential to describe the thermodynamic equilibrium.

This formalism is suitable for describing the dynamics of diffusion through major ionic channels. However, some currents, e.g., fast sodium current,  $I_{Na}$ , require a more precise description. Such description is done by estimating the ion flow  $j$ , due to membrane permeability  $P$ , via the solution of an electro-diffusion equation, assuming a constant field inside the channel [7, 9], rather than by the Ohm's law:

$$j = P \frac{zFU}{RT} \frac{C_o - C_i e^{zFU/RT}}{e^{y \frac{zFU}{RT}} - 1}. \quad (1.2)$$

It should be noted that currents through ionic pumps and exchangers, i.e.  $I_{NaK}$ ,  $I_{Ca,P}$ , and  $I_{NaCa}$  have to account for the change of protein conformation upon ions transfer according to the Michaelis–Menten kinetics.

The master differential equation for the transmembrane potential is as follows:

$$\begin{aligned} -C_m \frac{dU}{dt} = & I_{Na} + I_{Ca,L} + I_{Ca,T} + I_f + I_{Kr} + I_{Ks} + I_{to} + I_{sus} + I_{KACH} \\ & + I_{bNa} + I_{bCa} + I_{bK} + I_{NaK} + I_{NaCa} + I_{Ca,p} \end{aligned} \quad (1.3)$$

where  $I_{Na}$  is the fast sodium current;  $I_{Ca,T}$ ,  $I_{Ca,L}$  –  $Ca^{++}$  L and T type currents;  $I_f$  – hyperpolarization-activated current;  $I_{Kr}$  and  $I_{Ks}$  – rapid and slow delayed rectifying potassium current;  $I_{to}$ ,  $I_{sus}$  – 4-AP sensitive currents;  $I_{KACH}$  – ACh activated  $K^+$  current;  $I_{bNa}$ ,  $I_{bCa}$ ,  $I_{bK}$  – background currents;  $I_{NaK}$  – Na-K ATPase current;  $I_{NaCa}$  – Na-Ca exchanger current;  $I_{Ca,p}$  –  $Ca^{++}$  pump current. The parameters of the model related to membrane currents can be found in [23].

In addition, we have accounted for the change in the intracellular and intracellular sodium, potassium and calcium ion concentration by estimating a net sum of appropriate transmembrane electric currents:  $dC/dt = I(U, C, p)/(zFV)$  and  $dC_{Ca}/dt = C_v(U, C, p) - C/\tau(U, C)$ .

The calcium ion concentration was calculated at the four different cell compartments: myoplasm, calcium uptake from myoplasm to network sarcoplasmic reticulum (NSR) by the SERCA-2 pump, concentration in junctional sarcoplasmic reticulum (JSR) to where calcium ions diffuse from NSR, and  $Ca^{++}$  concentration in the dyadic subspace. The model also accounts for calcium bufferization by troponin-C, calmodulin and calsequestrin. The parameters of the model related to the processes in the SR are described in [11].

The ACh effect on the action potential is modelled by the inhibition of L-type calcium currents, activation of the ACh-dependent potassium current, and a shift in the activation curve of the hyperpolarization-activated current. The ACh concentration are within the physiological range [24].

A detailed list of a single sinoatrial node (SAN) pacemaker-cell model equations and numeric constants can be found in [2–4, 11, 23, 24].

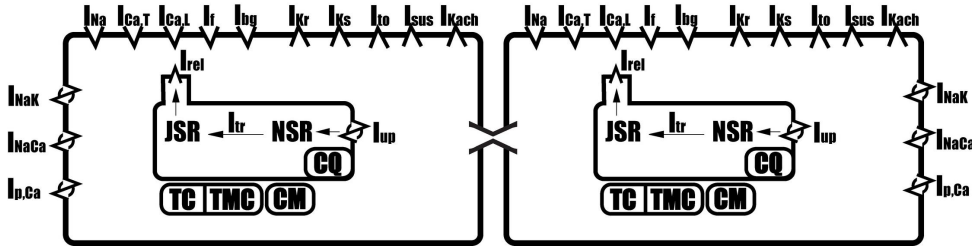


**Figure 1.** Scheme of two SAN pacemaker cells coupled electrically via gap junctions. Depicted membrane currents and sarcoplasmic reticulum elements are listed in the text.

In addition to central and peripheral cells [23] we have also modelled intermediate cells, linearly interpolating the parameters  $p(i_{ct}) = p_c + i_{ct} p_p$ , where  $i_{ct}$  is the cell type, varying from 0 to 1;  $p_c$  and  $p_p$  are the respective extremes (central and peripheral) of the parameter values [19]. The ionic model of the atrial tissue used to simulate the surrounding SAN tissue is based on similar principles and is described in detail in [12].

The interaction of cardiocytes via gap junctions (Fig.1) was simulated by assuming gap junctions as constant-resistance conductors. Gap junction conductivities inside the SAN were assumed 4.0 or 7.5 nS, which is consistent with the experiment [21], and large enough to synchronize the cells [19]. The junction conductivity between the atrium cells was 175 nS, which is consistent with the data from [22]. The conductivity on the boundary of the SAN and atrium was assumed 70 nS.

To estimate the number of leading centers and their density (Fig. 3) we assumed a cell A to be a leading center if at the moment  $t$ , a membrane potential  $U_A(t) > -30$  mV  $> U_B(t)$ , while  $U_A(t - dt) < -30$  mV, for any cell B, so that  $x(B) - x(A) < 0.21$  mm,  $y(B) - y(A) < 0.21$  mm,  $z(B) - z(A) < 0.21$  mm.

We have simulated a medium of  $50 \times 50 \times 20$  cells, which corresponds to a slab of approximately  $3.5 \times 3.5 \times 1.4$  mm of SAN tissue. Central, peripheral and intermediate pacemakers were randomly uniformly distributed within the simulated region, i.e., the probability density function  $p(i_{ct}) = 1$  for any cell within the tissue. An impermeable wall was used as the boundary condition. To simulate the effect of surrounding atrium tissue, the simulated region was extended by two slabs of atrium ( $50 \times 100 \times 20$  cells).

Differential equations were integrated using the Euler method. Differential equations of simple relaxation (1.1c) were integrated directly assuming constant coefficients during a time step:

$$\alpha(t + dt) = \alpha_\infty - (\alpha_\infty - \alpha) \exp(-dt/\tau). \quad (1.4)$$

The numeric values of the  $\alpha_\infty$ , and  $\tau$  for sodium, potassium and calcium currents can be found in [23].

We used time steps of  $10^{-5}$  s or less to adequately simulate the fastest sodium current. It should be noted that such small time steps are not due to the restriction of the simple method of integration applied, but result from the physical nature of

the simulated processes. The transmembrane potential, ion concentrations and other parameters were assumed spatially uniform within a single cell, i.e., the spacial steps correspond to the size of cardiocytes: to  $70\ \mu\text{m}$  in the case of SAN cells [5], to  $100\ \mu\text{m}$  in the case of atrial cells [18]. Thus we have simulated a medium composed of cardiocytes.

The 3D simulations were performed on a MIPT-60 cluster supercomputer situated at the Moscow Institute of Physics and Technology.

## 2. Results

To simulate synchronized oscillations, we assumed a uniform phase distribution as the initial condition, i.e. all cells within the SAN were synchronized at  $t = 0$  (Fig. 2a). We have observed thus artificially imposed all-cell-synchronized system to be unstable, in a short time numerous leading centers are formed (Figs. 2b and 2c). After a few oscillations the system evolves to a new equilibrium and the density of the leading centers gradually decreases with time (Fig. 3). After 100 s (Fig. 2d) we superfused the system with ACh, assuming the concentration of ACh rise to  $40\text{nM/L}$  at every point of the system. This resulted in a distortion of the propagation patterns (see Figs. 2d and 2f compared to Fig. 2c) and a migration of the dominating leading center (Fig. 4). Surprisingly we did not observe smooth diffusion-like migration, rather a leap-like manner of the leading center migration, which looked as if it was switched off at one place to appear in another, eventually in a distant place. The length of such leaps was up to  $3.2\ \text{mm}$ , which is comparable to the size of the SAN. The cause of this effect is that there are always plenty of latent leading centers in the tissue (Fig. 3) and a leap corresponds to the transformation of a latent center into an acting leading center. One can also see that the process of the leading center migration takes about 40 s, while the characteristic time of the change of the whole pattern of action potential propagation is much longer (Figs. 2e and 2f).

After ACh was eliminated from the system ( $t = 200\ \text{s}$ , Fig. 2g), the dominating leading center migrated back to its original place in 10 s (Figs. 2h and 2i). It is interesting to note that the backward migration path did not coincide with the forward migration path, as it was observed recently in 2D simulations [20].

The period of oscillations of the dominating leading center is shown in Fig. 5. The period quickly grew from  $0.27$  to  $0.53\ \text{s}$  after ACh superfusion ( $t = 100\ \text{s}$ ), and then gradually decreased and settled at  $0.45\ \text{s}$ . Thus we have observed a classical negative chronotropic effect of ACh [24]. After ACh was washed out ( $t = 200\ \text{s}$ ), the period quickly decreased down to  $0.22\ \text{s}$  and then gradually restored its original value of  $0.27\ \text{s}$ . It should be noted that in this figure we show the period measured at the center of the dominating leading center; the period at the other locations of the medium was settled close to the values shown in the figure, the transients died out during a single oscillation.

Recent studies have shown that a high ACh concentration resulted in the pacemaker loosing its spontaneous activity, but retaining its excitability [4]; experiments have confirmed these findings [1,6]. To simulate this effect in a 3D tissue we applied

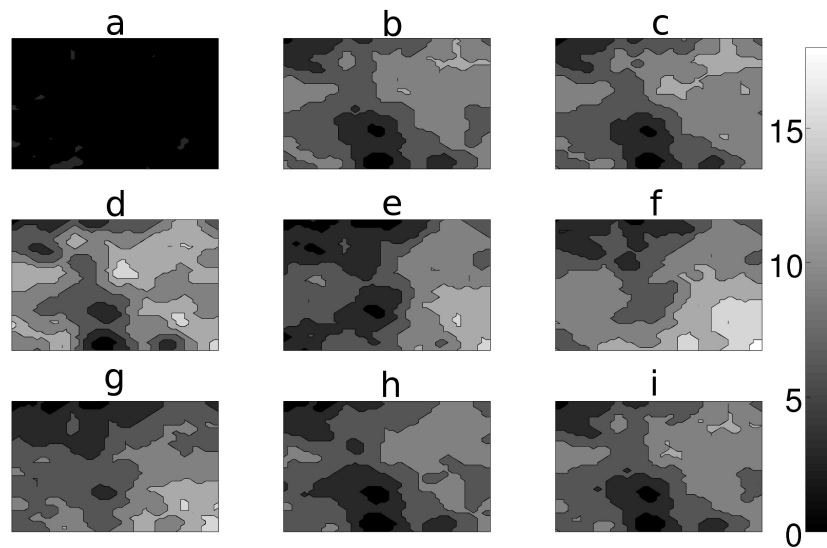


**Figure 2.** Chronotopographic maps of excitation propagation in the SAN. A 2D cut along Z-axis ( $z=15$ ) of 3D simulations is shown. Figures (a–i) are the snapshots at the moments of 0.165 s, 40.044 s, 99.006 s, 100.362 s, 140.358 s, 199.287 s, 200.211 s, 240.231 s, 299.223 s; 40 nM/L ACh was applied at 100 s and was eliminated at 200 s. The size of specimen in each subfigure is  $3.5 \times 3.5$  mm. The vertical scale at the right: time of excitation propagation ( $t$ , ms).

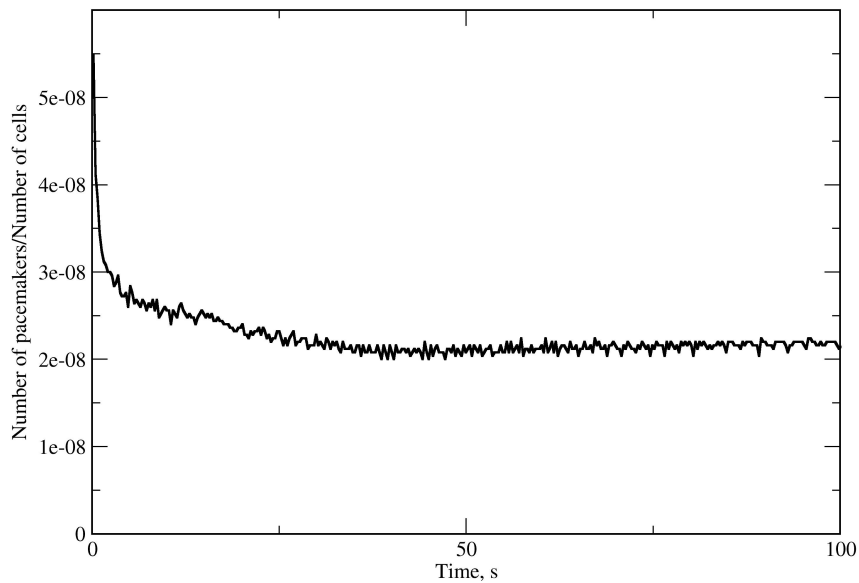


**Figure 3.** Evolution of pacemaker density in the SAN. Note that the initially large number of pacemakers significantly drops during the first few seconds.

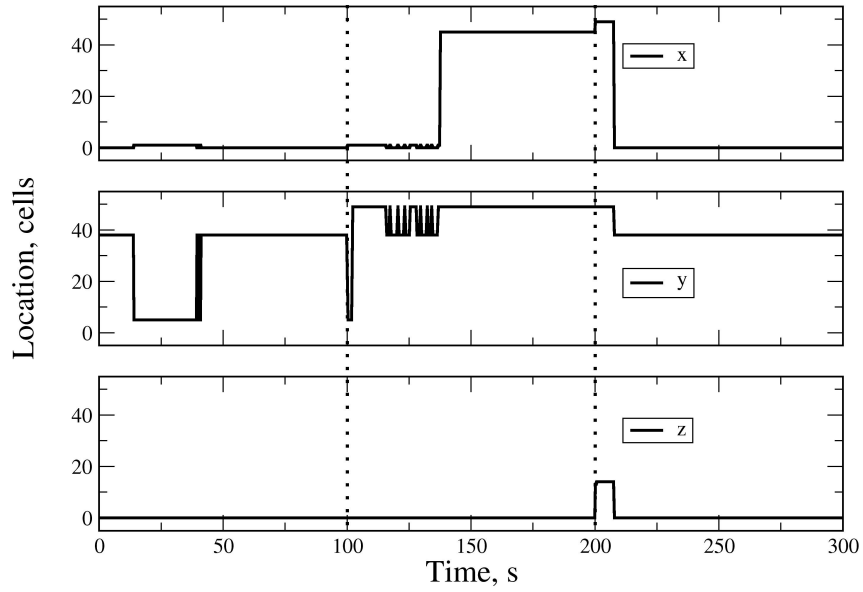


**Figure 4.** Location of the dominating leading center. Vertical dotted lines at 100 and 200 s – moments of 40 nM/L ACh superfusion and wash out.

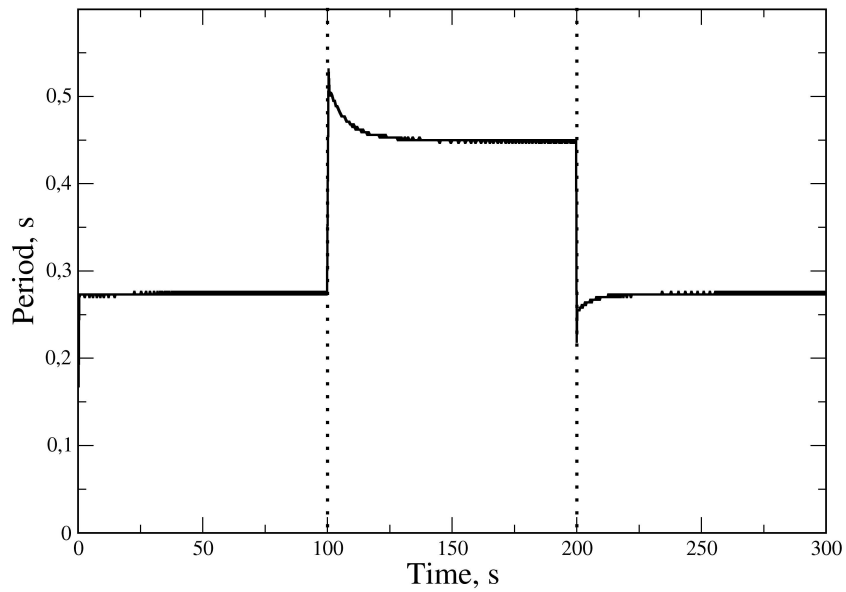


**Figure 5.** The effect of ACh superfusion on the period of the dominating leading center. Dotted lines at 100 and 200 s – moments of 40 nM/L ACh superfusion and wash out.

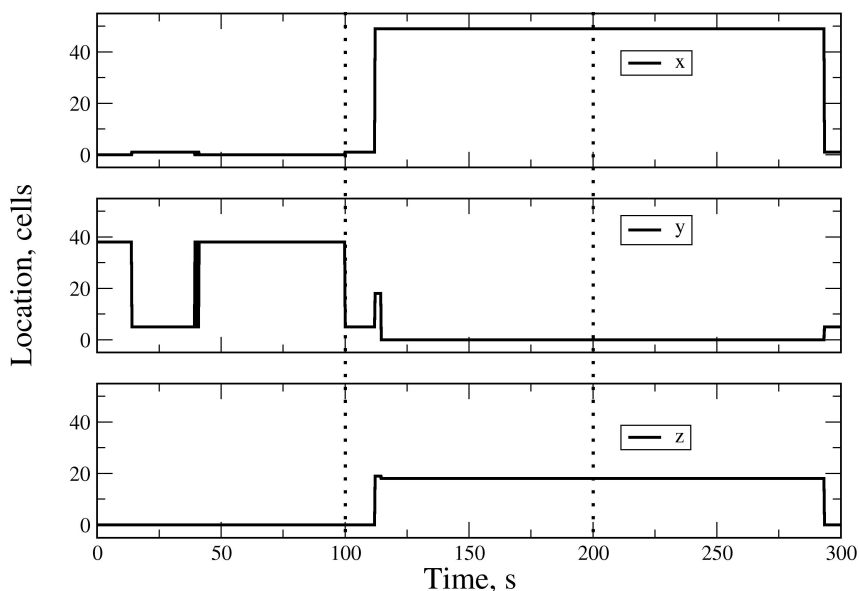


**Figure 6.** Location of the dominating leading center. Vertical dotted lines at 100 and 200 s – moments of 1 mM/L local ACh application and wash out.

1  $\mu$ M/L ACh locally, simulating a release of ACh from a locus of vagal nerves. Thus high concentration of ACh affected a ball of tissue 0.7 mm in diameter.

This local application of ACh resulted in the migration of the dominating leading center (Fig. 6) in a manner similar to its migration during ACh superfusion (Fig. 2). The migration took less time (about 15 s) and, unlike the case of ACh superfusion, the leading center did not return to its original place even 100 s after the ACh was washed out (Fig. 6). Surprisingly, ACh did not affect the period of oscillations of the medium outside the area where ACh was applied: it remained 0.27 s, while the SAN was driven by a leading center outside the site of ACh application.

In Fig. 7 one can see the propagation of the action potential; a site of ACh application is clearly seen in Fig. 7b (marked by the arrow). In contrast to the normal medium or the medium superfused by ACh (Fig. 2) where there was no clear preferred direction of the action potential propagation, in the case of local ACh application the potential was initiated in a distant part relative to the site of ACh application, and a wave with a rather smooth front propagated from there to the site of ACh application (Figs. 7c and 7d). This pattern persisted even 80 s after ACh was completely eliminated (Figs. 5e and 5f), demonstrating the effect of memory.

We have observed that even a random uniform distribution of pacemaker cells in both aforementioned simulations resulted in the leading centers tending to stay near the border of the tissue (Figs. 4 and 6). That might be a boundary effect: we used an impermeable wall as the boundary condition. Thus we suggest that the processes near the SAN boundary may crucially affect the location of the leading centers

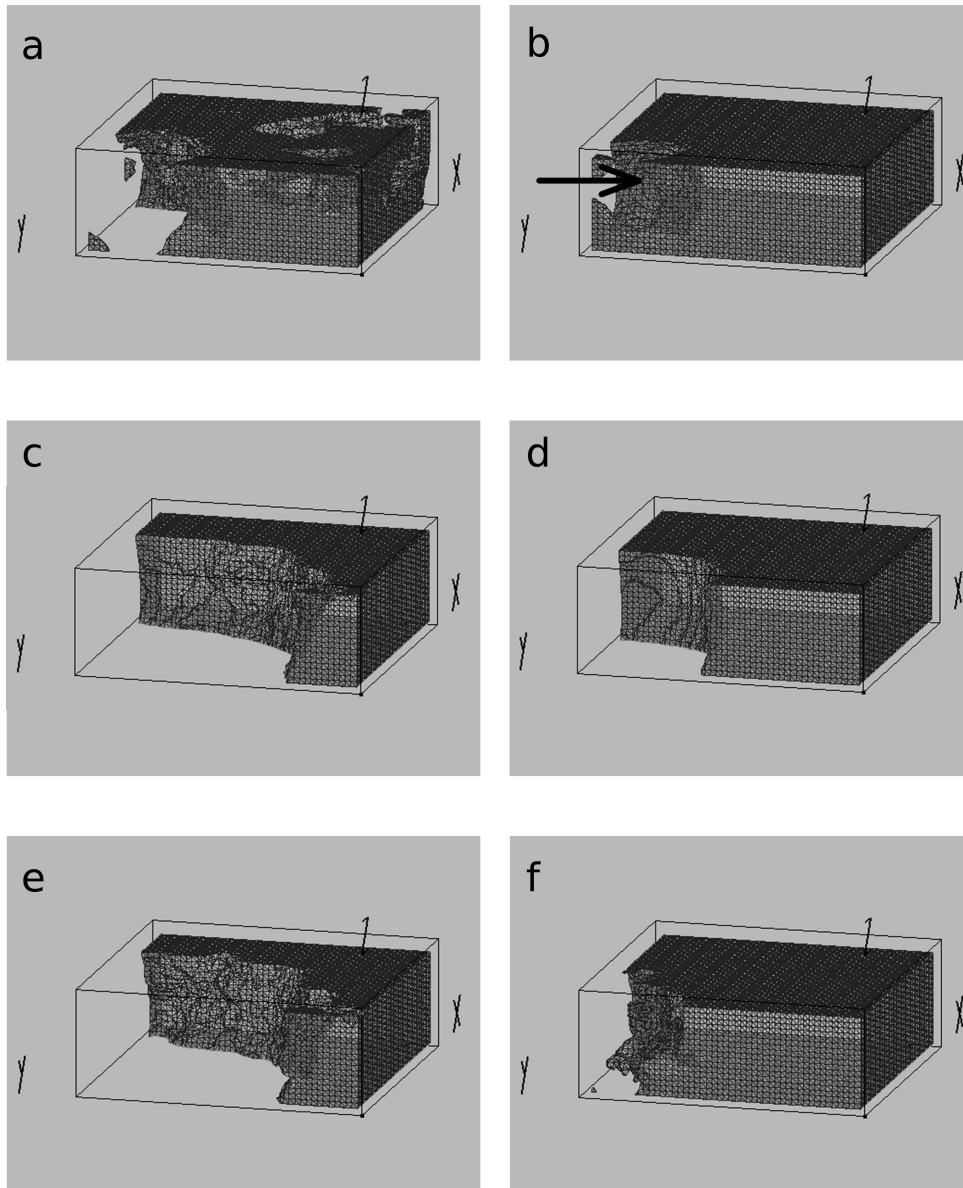


**Figure 7.** Propagation as a result of local application of the ACh front of action potential is shown. (a–f) are snapshots at 100.123 s, 100.138 s, 180.183 s, 181.013 s, 170.078 s, 170.093 s. 1 mM/L ACh is applied from 100 to 200 s. (a, b) – complex wave patterns, the arrow marks the site of ACh application (empty region in (b)); (c,d) – smooth wave with a constant-shaped front propagates from the farmost-right corner of tissue to the nearest-left corner of tissue; (e, f) – after ACh wash-out the wave still follows the same path, but its front shape changes while the wave propagates.

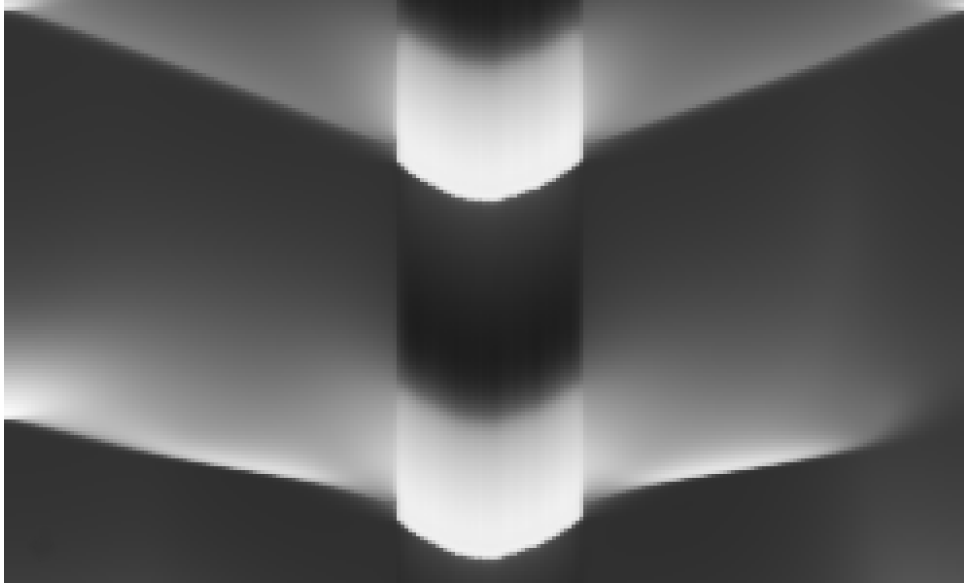


**Figure 8.** Propagation along SAN (center) and along the surrounding atrial tissue (left and right). Vertical axis stands for time from 98.7 s to 99.15 s; horizontal axis – space, a 1D section is along x-axis ( $y = 25, z = 10$ ). White color corresponds to depolarization, black to repolarization. Note a clear boundary between the SAN and the atrial tissue where a delay of propagation occurs.

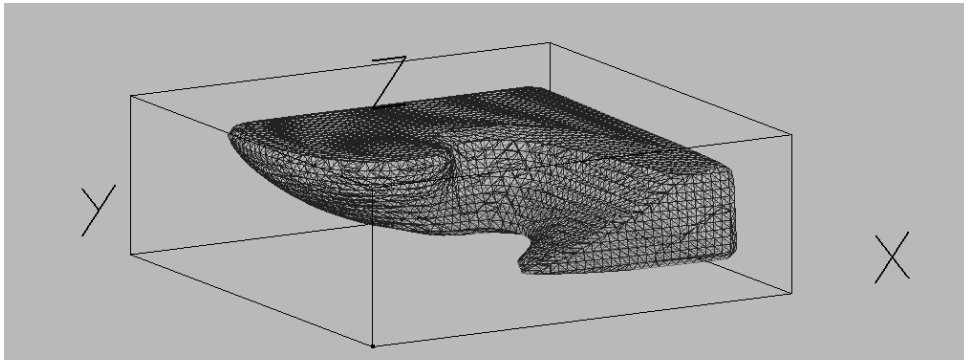


**Figure 9.** Rotating wave, reentry inside the SAN 150 ms after the initiation.

inside the SAN. We attached two slabs of atrium tissue alongside the SAN tissue as natural boundary conditions to simulate the propagation which might occur along crista terminalis. In Fig. 8 one can see two successive waves: the action potential has been initiated in the center of the SAN, in about 30 ms it reaches the border of the SAN and, after a delay of about 15 ms, propagates into the atrium slab along the X-axis.

Upon applying special initial conditions, namely, a helical surface for the phase of oscillations in cylindrical coordinates at  $t = 0$ :  $\text{phase} = \phi_0 + z\pi/z_{\max}$ , we have observed a rotating vortex inside the SAN (Fig. 9). The dynamics of such formation is extremely important for understanding atrial fibrillation as discussed below.

### 3. Discussion

Computer simulation of 3D electrical activity in the SAN and atria is a unique modern non-invasive tool to study the dynamics in a detailed way that currently cannot be achieved experimentally. Some general aspects and approaches to such modelling can be found in [17]. In the current work we have concentrated on the particular issues of the heart rhythm formation in the SAN, the effect of ACh on the leading center migration and on the formation of the local functional block that may become a precursor to a reentry and neurogenic atrial fibrillation.

It should be noted that the parameters of cell distribution in SAN tissue and the exact way of cellular organization in the SAN are still unknown [13, 25]. In this work, for the sake of simplicity, we have used the uniform random distribution of central, peripheral, and intermediate pacemaker cells. Such distribution of pacemakers reflects the basic properties of SAN tissue, as well as the cultured tissue of myocytes.

A phenomenon of migration of the leading center in the SAN has attracted attention since its discovery by Meek and Eyster [14]. It has been mostly studied experimentally [1]. We have recently succeeded in computer simulations of the phenomenon in a 2D model [20], and now in 3D (Figs. 2 and 4). We have observed that the paths of forward (upon ACh superfusion) and backward (upon ACh wash out) migration do not coincide, despite the fact that the dominating leading center does return back to its original location (Fig. 4). This was recently shown in 2D [20] and is now confirmed in 3D simulations. This emphasizes the fact that the process of the leading center migration is of complex nature and cannot be considered simply as the suppression and restitution of an acting leading center.

Note that the effect of ACh on wave patterns in 3D and in 2D is similar, but not identical. For example, consider the propagation as a result of local application of ACh (Fig. 7): an application of a high concentration of ACh in a 2D disk has completely interrupted propagation, while an application of a high concentration of ACh in a 3D ball (Fig. 7) does not have such a drastic effect due to the obvious differences in 2D and 3D space geometry. It is also worth noting that the number of leading centers within 3D tissue (Fig. 3) was larger than within 2D tissue. As the result, while the excitation of 2D tissue ( $50 \times 50$  cells) took about 50–70 ms, it took less than 20 ms in 3D simulations ( $50 \times 50 \times 20$  cells). And, of course, 3D simulations are more realistic.

In our simulations (as well as in the experiments [1]) the migration of the leading center is a slow process lasting dozens of seconds. Note that neither of the differential equations of the model (1.1c) describing membrane dynamics of the Hodgkin type has such long time constants. The observed characteristic time of mi-

gration (Figs. 4 and 5) may indicate that migration is crucially affected by slow changes in intracellular ion homeostasis [2]. Indeed, it was shown that the application of ACh, besides an immediate chronotropic effect, resulted in slow (dozens of seconds) changes in the intracellular concentrations of the major ions: sodium and potassium [2]. These changes affect the functioning of sodium, potassium and other channels, thus resulting in slow pacemaker-cell frequency shifts. Local differences in oscillation frequencies is the major factor that results in the formation (generally fast) of leading centers, suppressing (generally slow) the neighbour latent pacemakers.

To simulate the propagation of the excitation from the SAN into the atrium we have extended the model of SAN tissue by two slabs of atrium cells. This allowed us to simulate propagation that occurs in the heart along crista terminalis and to study the effect of the surrounding atrial tissue on the location of leading centers in the SAN. We have found that the effect of boundary conditions is crucial: simulating isolated SAN tissue we observed that the leading centers tended to locate near the boundary, and when the atria are attached, the preferred location of the leading centers is shifted to the midst of the SAN tissue. To explain the effect we should recall that atrial cells are larger than SAN pacemaker cells and that atrial cells at equilibrium are negatively charged to  $-70$  mV. Thus, part of the charge generated by transmembrane currents of the peripheral SAN cells was consumed by the atrial cells, which makes the depolarization of SAN pacemakers slower and, therefore, the location of the leading center shifts toward the center of the SAN. The leakage of charge is also responsible for the propagation delay on the boundary between the SAN and the atrium (Fig. 8). This may also be the reason of larger fast-oscillating cells location on the periphery of the SAN: the stronger pacemaker activity in the cells of the SAN periphery can help to overcome the suppressive effect of the right atrium on the overall SAN automaticity [13].

An interesting unsolved problem is whether a vortex-like reentry pattern occurs inside the SAN under pathological conditions. Such patterns are known to be precursors of dangerous arrhythmia in ventricles and in atria. As for the SAN, the literature data are contradictory and a discussion has been open since the experiments by Hutter and Trautwein [10]. The role of ACh in the effect has been addressed in simulations with a simple cellular automata model of a frog myocardium [16]. However, it is not clear whether this phenomenon exists in mammals (see [15] for discussion). In the current work we have made a first attempt to simulate such a reentry in a realistic 3D model of SAN tissue (Fig. 9). To succeed, we have applied rather artificial initial conditions, i.e., a helical surface. To clarify how common is this phenomenon, and to determine its dynamics, further simulations are needed.

## References

1. D. V. Abramochkin, V. S. Kuzmin, G. S. Sukhova, and L. V. Rosenshtraukh, Modulation of rabbit sinoatrial node activation sequence by acetylcholine and isoproterenol investigated with optical mapping technique. *Acta Physiol. (Oxf.)* (2009) **196**, No. 4, 385–394.
2. R. R. Aliev and L. M. Chailakhyan, Study of the effect of acetylcholine on intracellular

- homeostasis of true pacemaker cells of rabbit sinus node using computer simulation. *Doklady Biochem. Biophys.* (2005) **402**, No. 1, 236–239.
3. R. R. Aliev, V. V. Fedorov, and L. V. Rosenshtrakh, Simulation of ACh effects on ionic current of primary and subsidiary pacemakers single cells of rabbit sinoatrial node. *Doklady Biolog. Sci.* (2004) **397**, No. 5, 697–700.
  4. R. R. Aliev, V. V. Fedorov, and L. V. Rosenshtrakh, Study of the effect of acetylcholine on the excitability of true pacemaker cells of rabbit sinus node using computer simulation. *Doklady Biolog. Sci.* (2005) **402**, No. 4, 548–550.
  5. M. R. Boyett, H. Honjo, I. Kodama, M. K. Lancaster, M. Lei, H. Musa, and H. Zhang, The sinoatrial node: cell size does matter. *Circ. Res.* (2007) **101**, No. 7, e81–e82.
  6. V. V. Fedorov, W. J. Hucker, H. Dobrzynski, L. V. Rosenshtrakh, and I. R. Efimov, Postganglionic nerve stimulation induces temporal inhibition of excitability in rabbit sinoatrial node. *Amer. J. Physiol.* (2006) **291**, No. 2, H612–H623.
  7. D. E. Goldman, Potential, impedance, and rectification in membranes. *J. Physiol.* (1943) **27**, No. 1, 37–60.
  8. A. L. Hodgkin and A. F. Huxley, A quantitative description of membrane current and its application to conduction and excitation in nerve. *J. Physiol.* (1952) **117**, No. 4, 500–544.
  9. A. L. Hodgkin and B. Katz, The effect of sodium ions on the electrical activity of the giant axon of the squid. *J. Physiol.* (1943) **108**, No. 1, 37–77.
  10. O. F. Hutter and W. Trautwein, Vagal and sympathetic effects on the pacemaker fibers in the sinus venosus of the heart. *J. Gen. Physiol.* (1956) **39**, No. 5, 715–733.
  11. Y. Kurata, I. Hisatome, S. Imanishi and T. Shibamoto, Dynamical description of sinoatrial node pacemaking: improved mathematical model for primary pacemaker cell. *Amer. J. Physiol.* (2002) **283**, No. 5, H2074–H2101.
  12. D. S. Lindblad, C. R. Murphey, J. W. Clark, and W. R. Giles, A model of the action potential and underlying membrane currents in a rabbit atrial cell. *Amer. J. Physiol.* (1996) **271**, No. 4, H1666–H1696.
  13. M. E. Mangoni and J. Nargeot, Genesis and regulation of the heart automaticity. *Physiol. Rev.* (2008) **88**, No. 3, 919–982.
  14. W. J. Meek and J. A. E. Eyster, Experiments on the origin and propagation of the impulse in the heart: IV. the effect of vagal stimulation and of cooling on the location of the pacemaker within the sino-auricular node. *Amer. J. Physiol.* (1914) **34**, No. 4, 368–383.
  15. A. V. Rozenshtrakh, R. R. Aliev, G. Beloshapko, and A. V. Iushamnova, Experimental and theoretical analysis of the role of cholinergically induced local non-excitability in atrial fibrillation and flutter. *Kardiologi.* (2007) **47**, No. 4, 4–17 (in Russian).
  16. L. V. Rozenshtrakh, A. V. Kholopov, and A. V. Iushmanova, Vagus inhibition—cause of the formation of closed pathways of excitation conduction in auricles. *Biofizika* (1970) **15**, No. 4, 690–700 (in Russian).
  17. G. Seemann, C. Höper, F. B. Sachse, O. Dössel, A. V. Holden, and H. Zhang, Heterogeneous three-dimensional anatomical and electrophysiological model of human atria. *Phil. Trans. R. Soc. A* (2006) **364**, No. 1843, 1465–1481.
  18. R. M. Shaw and Y. Rudy, Ionic mechanisms of propagation in cardiac tissue. roles of the sodium and L-type calcium currents during reduced excitability and decreased gap junction coupling. *Circ. Res.* (1997) **81**, No. 5, 727–741.
  19. R. Syunyaev and R. Aliev, Modelling of the influence of gap-junction coupling on synchronization of central and peripheral sinoatrial node cells. *Biophys.* (2009) **54**, No. 1, 58–60.

20. R. Syunyaev and R. Aliev, Computer simulations of pacemaker shift in the sinoatrial node. *Biophys.* (2010) **55**, No. 6, 1025–1029.
21. S. Verheule, M. J. Van Kempen, S. Postma, M. B. Rook, and H. J. Jongsma, Gap junctions in the rabbit sinoatrial node. *Amer. J. Physiol.* (2001) **280**, No. 5, H2103–H2115.
22. S. Verheule, M. J. Van Kempen, P. H. Te Welscher, B. R. Kwak, and H. J. Jongsma, Characterization of gap junction channels in adult rabbit atrial and ventricular myocardium. *Circ. Res.* (1997) **80**, No. 5, 673–681.
23. H. Zhang, A. V. Holden, I. Kodama, H. Honjo, M. Lei, T. Varghese, and M. R. Boyett, Mathematical models of action potentials in the periphery and center of the rabbit sinoatrial node. *Amer. J. Physiol.* (2000) **279**, No. 1, H397–H421.
24. H. Zhang, A. V. Holden, D. Noble, and M. R. Boyett, Analysis of the chronotropic effect of acetylcholine on sinoatrial node cells. *J. Cardiovasc. Electrophysiol.* (2002) **13**, No. 5, 465–474.
25. H. Zhang, A. V. Holden and M. R. Boyett, Gradient model versus mosaic model of the sinoatrial node. *Circulation* (2002) **103**, No. 4, 584–588.